

# Simple analytical–statistical models (ASMs) for mean annual permafrost table temperature and active-layer thickness estimates

Tomáš Uxa<sup>1,2</sup>, Filip Hrbáček<sup>2</sup>, and Michaela Kňázková<sup>2</sup>

<sup>1</sup>Institute of Geophysics, Czech Academy of Sciences, Prague, Czech Republic

<sup>2</sup>Polar-Geo-Lab, Department of Geography, Faculty of Science, Masaryk University, Brno, Czech Republic

**Correspondence:** Tomáš Uxa (uxa@ig.cas.cz)

**Abstract.** A number of models have been developed for estimating the mean annual permafrost table temperature (MAPT) and active-layer thickness (ALT). These tools typically require at least a few ground physical properties as their input parameters in addition to air or ground temperatures. However, ground physical properties are frequently unavailable or unrepresentative and therefore need to be estimated, which introduces uncertainties into model outputs. Hence, we devised two simple analytical–statistical models (ASMs) for MAPT and ALT, which are driven solely by thawing and freezing indices from two depth levels within the active layer, while no ground physical properties are required. ASMs reproduced MAPT and ALT in the Earth’s major permafrost regions with the total mean errors of less than 0.05 °C and 89%, respectively. This is similar or better than other analytical or statistical models, which suggests that ASMs can be useful tools for estimating MAPT and ALT under a wide range of environmental conditions.

## 10 1 Introduction

Of ~11 % of the Earth’s exposed land surface underlain by permafrost (Obu, 2021), most seasonally thaws from the ground surface to a depth of up to several meters and then completely refreezes, which is mainly controlled by climate conditions and ground physical properties (Bonnaventure and Lamoureux, 2013). This superficial active layer greatly influences the energy and mass transfer between the underlying permafrost, ground surface and the atmosphere, and is therefore critical for the dynamics of hydrological, geomorphic, pedogenic, biological and/or biogeochemical processes including greenhouse gas fluxes, as well as for human infrastructure in permafrost regions (e.g., Grosse et al., 2016; Walvoord and Kurylyk, 2016; Hjort et al., 2022). As climate is a first-order control on ground temperatures and thaw depth (Wang et al., 2019; Smith et al., 2022), the thermal state of permafrost and the thickness of the active layer have attracted a huge interest over recent decades because they are important indicators of how the climate system is evolving (Li et al., 2022; Hrbáček et al., 2023b). Climate change has provoked permafrost warming and active-layer thickening at a global scale (Noetzli et al., 2024; Smith et al., 2024), which can have severe consequences on landscape and ecosystem stability as well as infrastructure integrity. Carbon release due to permafrost degradation is likely to trigger feedback mechanisms with impacts on the Earth’s climate system (Lawrence et al., 2015; Schuur et al., 2022). The permafrost and active-layer monitoring is therefore of utmost scientific and societal importance (Brown et al., 2000; Biskaborn et al., 2015).

25 The thermal state of permafrost and the thickness of the active layer have been investigated by semi-continuous temperature measurements using data loggers with temperature sensors distributed in vertical arrays across the active layer and near-surface permafrost (e.g., Biskaborn et al., 2015; Noetzli et al., 2021), by periodic or semi-continuous geophysical measurements using electric, electromagnetic or seismic methods (e.g., Hauck, 2002; Farzamian et al., 2020), or by periodic thaw-depth measurements using physical probing with rigid rods or thaw-tube readings (e.g., Burn, 1998; Bonnaventure and Lamoureux, 30 2013). Of these methods, temperature measurements using data loggers are the most convenient in terms of accuracy, temporal resolution and/or logistics, which is well suitable for remote and poorly accessible permafrost regions that have limited or no technical infrastructure (Biskaborn et al., 2015; Streletskiy et al., 2022). However, ground temperatures are frequently measured only in the active layer, and therefore the permafrost temperatures and the active-layer thickness need to be estimated in these situations. This has been done using either statistical methods or numerical and analytical models of various complexity (e.g., 35 Riseborough, 2008; Riseborough et al., 2008; Bonnaventure and Lamoureux, 2013; Aalto et al., 2018).

Of these solutions, analytical models in particular have become popular for estimating the mean annual temperature at the top of permafrost (hereafter referred to as the mean annual permafrost table temperature, MAPT) (Garagulya, 1990; Romanovsky and Osterkamp, 1995; Smith and Riseborough, 1996) and the active-layer thickness (ALT) (Neumann, c. 1860; Stefan, 1891; Kudryavtsev et al., 1977) because of their simplicity, small number of input parameters, computational efficiency and yet 40 sufficient accuracy, which is advantageous for diverse permafrost regions and environmental settings (e.g., Anisimov et al., 1997; Nelson et al., 1997; Zhao et al., 2017; Obu et al., 2019, 2020). These tools typically require at least a few ground physical properties, such as thermal conductivity, heat capacity, water content or bulk density, as their input parameters in addition to air or ground temperatures. However, ground physical properties are frequently unavailable or unrepresentative and therefore need to be estimated, which introduces uncertainties into model outputs. But even *in situ* observations of ground 45 physical properties may not guarantee accurate model outputs either, as these properties are usually measured annually or less frequently and are then treated as constants in models, regardless of their temporal variability, which can be considerable (e.g., Gao et al., 2020; Hrbáček et al., 2023a; Li et al., 2023; Kňázková and Hrbáček, 2024; Wenhao et al., 2024).

Here, we devise two novel analytical–statistical models (ASMs) for MAPT and ALT, which are driven solely by thawing and freezing indices from two depth levels within the active layer. ASMs are primarily intended to be used for MAPT or 50 ALT estimates where ground temperature measurements are too shallow and MAPT or ALT therefore cannot be determined directly, while no information on ground physical properties exists. We evaluate ASMs against *in situ* ground temperature measurements from the Earth’s major permafrost regions, and we discuss their performance, advantages and limitations.

## 2 Model derivation

### 2.1 Mean annual permafrost table temperature

55 MAPT [°C] can be calculated using the TTOP model (Romanovsky and Osterkamp, 1995; Smith and Riseborough, 1996), which assumes that the ratio of thawed and frozen thermal conductivity and the effects of latent heat produce the difference between MAPT and the mean annual ground surface temperature (thermal offset). The TTOP formula for permafrost conditions

(MAPT  $\leq 0$  °C) is as follows (Romanovsky and Osterkamp, 1995; Smith and Riseborough, 1996)

$$\text{MAPT} = \frac{\frac{k_t}{k_f} I_{ts} - I_{fs}}{P}, \quad (1)$$

60 where  $k_t$  [ $\text{W m}^{-1} \text{K}^{-1}$ ] and  $k_f$  [ $\text{W m}^{-1} \text{K}^{-1}$ ] is the thawed and frozen thermal conductivity, respectively, that defines the thermal conductivity ratio,  $I_{ts}$  [ $^{\circ}\text{C d}$ ] and  $I_{fs}$  [ $^{\circ}\text{C d}$ ] is the ground surface thawing and freezing index, respectively (both assumed in absolute values), and  $P$  [365 d] is the length of one year.

However, Eq. (1) can work with thawing and freezing index measured at any depth within the active layer (Riseborough, 2004). This is highly convenient because ground surface temperatures are difficult to measure due to radiative and convective energy fluxes and problematic fixing of temperature sensors exactly at the ground surface (Riseborough, 2003). Using ground temperatures measured at two depth levels within the active layer  $z_1$  and  $z_2$  ( $z_1 < z_2 < \text{ALT}$ ), MAPT can therefore be expressed as

$$\text{MAPT} = \frac{\frac{k_t}{k_f} I_{tz_1} - I_{fz_1}}{P}, \quad (2)$$

$$\text{MAPT} = \frac{\frac{k_t}{k_f} I_{tz_2} - I_{fz_2}}{P}, \quad (3)$$

70 where  $I_{tz_1}$  [ $^{\circ}\text{C d}$ ] and  $I_{fz_1}$  [ $^{\circ}\text{C d}$ ] is the thawing and freezing index at the depth  $z_1$ , and  $I_{tz_2}$  [ $^{\circ}\text{C d}$ ] and  $I_{fz_2}$  [ $^{\circ}\text{C d}$ ] is the thawing and freezing index at the depth  $z_2$ . This implies that Eq. (2) and (3) are equivalent:

$$\frac{\frac{k_t}{k_f} I_{tz_1} - I_{fz_1}}{P} = \frac{\frac{k_t}{k_f} I_{tz_2} - I_{fz_2}}{P}. \quad (4)$$

Solving Eq. (4) for the thermal conductivity ratio yields

$$\frac{k_t}{k_f} = \frac{I_{fz_1} - I_{fz_2}}{I_{tz_1} - I_{tz_2}}. \quad (5)$$

75 Equation (5) can be substituted for the thermal conductivity ratio in Eq. (2) and (3) as follows

$$\text{MAPT} = \frac{\frac{I_{fz_1} - I_{fz_2}}{I_{tz_1} - I_{tz_2}} I_{tz_1} - I_{fz_1}}{P}, \quad (6)$$

$$\text{MAPT} = \frac{\frac{I_{fz_1} - I_{fz_2}}{I_{tz_1} - I_{tz_2}} I_{tz_2} - I_{fz_2}}{P}. \quad (7)$$

Simplifying Eq. (6) and (7) then produces the same formula for MAPT:

$$\text{MAPT} = \frac{I_{fz_1} I_{tz_2} - I_{fz_2} I_{tz_1}}{I_{tz_1} - I_{tz_2}}. \quad (8)$$

80 Substantially, Eq. (8) implies that MAPT can be simply estimated using thawing and freezing indices from two depth levels within the active layer alone, that is, without knowing the thermal conductivity ratio.

Since Eq. (8) was derived from Eq. (1), it has a physical basis (cf. Romanovsky and Osterkamp, 1995). However, it can be shown that it is in principle a linear extrapolation of the freezing index to the depth, where the thawing index becomes zero, and dividing it by the length of one year. Using the same notation as before, this can be expressed as

$$85 \quad \frac{I_{fz_1} - I_{f_{ALT}}}{I_{tz_1} - I_{t_{ALT}}} = \frac{I_{fz_1} - I_{fz_2}}{I_{tz_1} - I_{tz_2}}, \quad (9)$$

$$\frac{I_{fz_2} - I_{f_{ALT}}}{I_{tz_2} - I_{t_{ALT}}} = \frac{I_{fz_1} - I_{fz_2}}{I_{tz_1} - I_{tz_2}}, \quad (10)$$

where  $I_{t_{ALT}}$  [ $^{\circ}\text{C d}$ ] and  $I_{f_{ALT}}$  [ $^{\circ}\text{C d}$ ] represents the thawing and freezing index at the base of the active layer. Note that the slope of the relationship is determined by the thermal conductivity ratio. Solving Eq. (9) and (10) for  $I_{f_{ALT}}$  gives

$$-I_{f_{ALT}} = \frac{I_{fz_1} - I_{fz_2}}{I_{tz_1} - I_{tz_2}} (I_{tz_1} - I_{t_{ALT}}) - I_{fz_1}, \quad (11)$$

$$90 \quad -I_{f_{ALT}} = \frac{I_{fz_1} - I_{fz_2}}{I_{tz_1} - I_{tz_2}} (I_{tz_2} - I_{t_{ALT}}) - I_{fz_2}. \quad (12)$$

Since the thawing index at the base of the active layer is zero, Eq. (11) and (12) become equivalent to Eq. (6) and (7), respectively, when divided by the length of one year, and both simplify to Eq. (8). This documents that Eq. (8) can be derived in two alternative manners consisting of analytical and statistical procedures.

## 2.2 Active-layer thickness

95 ALT [m] can be calculated using the Stefan (1891) model, which builds on the premise that the conductive heat flux above the thaw front equals to the rate at which latent heat is absorbed as the thaw front propagates downwards. Its simplest form is as follows (Lunardini, 1981)

$$\text{ALT} = \sqrt{\frac{2k_t I_{ts}}{L\phi}}, \quad (13)$$

100 where  $L [3.34 \times 10^8 \text{ J m}^{-3}]$  is the volumetric latent heat of fusion of water and  $\phi [-]$  is the volumetric water content. Note that the thawing index must be multiplied by the scaling factor of  $86\,400 \text{ s d}^{-1}$ . As stated previously (Sect. 2.1), ground surface temperatures are difficult to measure (Riseborough, 2003), and therefore the Stefan model has commonly been forced by ground temperatures collected at some depth within the active layer. However, this has rarely been accounted for, although it has been shown to substantially affect the model outputs (Hrbáček and Uxa, 2020; Kaplan Pastřířková et al., 2023). Yet, it can be easily implemented as follows (Riseborough, 2003; Hayashi et al., 2007)

$$105 \quad \text{ALT} = z + \sqrt{\frac{2k_t I_{tz}}{L\phi}}, \quad (14)$$

where  $z$  [m] is the depth at which the thawing index  $I_{tz}$  [ $^{\circ}\text{C d}$ ] is measured. Using ground temperatures measured at two depth levels within the active layer  $z_1$  and  $z_2$  ( $z_1 < z_2 < \text{ALT}$ ), ALT can therefore be expressed as

$$\text{ALT} = z_1 + \sqrt{\frac{2k_t I_{tz_1}}{L\phi}}, \quad (15)$$

$$\text{ALT} = z_2 + \sqrt{\frac{2k_t I_{tz_2}}{L\phi}}. \quad (16)$$

110 This implies that Eq. (15) and (16) are equivalent:

$$z_1 + \sqrt{\frac{2k_t I_{tz_1}}{L\phi}} = z_2 + \sqrt{\frac{2k_t I_{tz_2}}{L\phi}}. \quad (17)$$

The vertical distance between  $z_2$  and  $z_1$  can be expressed as

$$z_2 - z_1 = \sqrt{\frac{2k_t I_{tz_1}}{L\phi}} - \sqrt{\frac{2k_t I_{tz_2}}{L\phi}}, \quad (18)$$

which simplifies to

$$115 \quad z_2 - z_1 = \sqrt{\frac{2k_t}{L\phi}} \left( \sqrt{I_{tz_1}} - \sqrt{I_{tz_2}} \right). \quad (19)$$

Subsequently rearranging Eq. (19) gives

$$\frac{z_2 - z_1}{\sqrt{I_{tz_1}} - \sqrt{I_{tz_2}}} = \sqrt{\frac{2k_t}{L\phi}}, \quad (20)$$

where the right-hand side corresponds to the so-called edaphic term (Nelson and Outcalt, 1987), which has been used to combine the thawed thermal conductivity and volumetric water content into a single variable in the modified Stefan model:

$$120 \quad \text{ALT} = E \sqrt{I_{ts}}, \quad (21)$$

where  $E$   ~~$[\text{m}^{\circ}\text{C d}^{-0.5}]$~~   $[\text{m}^{\circ}\text{C}^{-0.5} \text{d}^{-0.5}]$  denotes the edaphic term given by

$$E = \sqrt{\frac{2k_t}{L\phi}}. \quad (22)$$

Although Eq. (21) is equivalent to Eq. (13), it has frequently been preferred for estimating ALT because the edaphic term can be calibrated based on the relationship between ALT and thawing index, that is, without knowing the thawed thermal conductivity and volumetric water content (Nelson and Outcalt, 1987; Hinkel and Nicholas, 1995; Nelson et al., 1997; Anisimov et al., 2002; Shiklomanov and Nelson, 2002; Smith et al., 2009; Shiklomanov et al., 2010; Peng et al., 2023). The edaphic term can be implemented in Eq. (15) and (16) as follows

$$\text{ALT} = z_1 + E \sqrt{I_{tz_1}}, \quad (23)$$

$$\text{ALT} = z_2 + E \sqrt{I_{tz_2}}. \quad (24)$$

130 Substituting the left-hand side of Eq. (20) for the edaphic term in Eq. (23) and (24) yields

$$\text{ALT} = z_1 + \frac{z_2 - z_1}{\sqrt{I_{tz_1}} - \sqrt{I_{tz_2}}} \sqrt{I_{tz_1}}, \quad (25)$$

$$\text{ALT} = z_2 + \frac{z_2 - z_1}{\sqrt{I_{tz_1}} - \sqrt{I_{tz_2}}} \sqrt{I_{tz_2}}. \quad (26)$$

Simplifying Eq. (25) and (26) then produces the same formula for ALT:

$$\text{ALT} = \frac{z_2 \sqrt{I_{tz_1}} - z_1 \sqrt{I_{tz_2}}}{\sqrt{I_{tz_1}} - \sqrt{I_{tz_2}}}. \quad (27)$$

135 Substantially, Eq. (27) implies that ALT can be simply estimated using thawing indices from two depth levels within the active layer alone, that is, without knowing the thawed thermal conductivity and volumetric water content or the edaphic term.

Since Eq. (27) was derived from Eq. (13), it has a physical basis (cf. Lunardini, 1981). However, it can also be shown that it is in principle a linear extrapolation of the depth where the square root of the thawing index becomes zero (cf. Riseborough, 2003). This can be expressed as

$$140 \frac{\text{ALT} - z_1}{\sqrt{I_{tz_1}} - \sqrt{I_{t_{\text{ALT}}}}} = \frac{z_2 - z_1}{\sqrt{I_{tz_1}} - \sqrt{I_{tz_2}}}, \quad (28)$$

$$\frac{\text{ALT} - z_2}{\sqrt{I_{tz_2}} - \sqrt{I_{t_{\text{ALT}}}}} = \frac{z_2 - z_1}{\sqrt{I_{tz_1}} - \sqrt{I_{tz_2}}}. \quad (29)$$

Note that the slope of the relationship is determined by the edaphic term. Solving Eq. (28) and (29) for ALT gives

$$\text{ALT} = z_1 + \frac{z_2 - z_1}{\sqrt{I_{tz_1}} - \sqrt{I_{tz_2}}} \left( \sqrt{I_{tz_1}} - \sqrt{I_{t_{\text{ALT}}}} \right), \quad (30)$$

$$\text{ALT} = z_2 + \frac{z_2 - z_1}{\sqrt{I_{tz_1}} - \sqrt{I_{tz_2}}} \left( \sqrt{I_{tz_2}} - \sqrt{I_{t_{\text{ALT}}}} \right). \quad (31)$$

145 Since the thawing index at the base of the active layer is zero, Eq. (30) and (31) are equivalent to Eq. (25) and (26), respectively, and both simplify to Eq. (27). As with Eq. (8), this documents that Eq. (27) can also be derived in two alternative manners consisting of analytical and statistical procedures.

### 3 Model evaluation

ASMs for estimating MAPT and ALT were evaluated using *in situ* ground temperature measurements from the Earth's major  
 150 permafrost regions that differ in climate, permafrost zone, ground surface cover and/or ground physical properties and their distribution within the active layer to enhance the robustness of the model evaluation. Unlike manual thaw-depth measurements, such as those from the Circumpolar Active Layer Monitoring (CALM) network (Brown et al., 2000), ground temperature measurements with sensors distributed in vertical arrays across the active layer and near-surface permafrost provide high temporal and depth resolutions, which enable consistent determination of MAPT and ALT using a uniform procedure at all sites and ensure the homogeneity of the validation dataset.  
 155 Since the accuracy of ~~the observed ALT~~ these MAPT and ALT

values depends on the distance-between-spacing of the ground temperature sensors (Riseborough, 2003, 2008), we arbitrarily set their maximum spacing attempted to keep their maximum distances at 25 cm and 4050 cm for ALT of <1 m and >1 m, respectively. While this requirement excluded numerous sites, it ensured that the benchmark values for MAPT and ALT could be established as accurately as possible.

160 We collected ground temperature data for a total of 43-55 sites from monitoring networks and public databases of the Polar-Geo-Lab of the Masaryk University (MU) (e.g., Hrbáček et al., 2017a, b; Hrbáček and Uxa, 2020; Hrbáček et al., 2025), Global Terrestrial Network for Permafrost (GTN-P; <http://gtnpdatabase.org>), Natural Resources Conservation Service of the United States Department of Agriculture (USDA; <https://www.nrcs.usda.gov/resources/data-and-reports/soil-climate-research-stations>), Geophysical Institute Permafrost Laboratory of the University of Alaska Fairbanks (GI-UAF, <https://permafrost.gi.alaska.edu>),  
165 Yukon Permafrost Database (YPD, <https://service.yukon.ca/permafrost/>), Nordicana D of the Centre for Northern Studies (ND, <https://nordicana.cen.ulaval.ca/en/>), and National Tibetan Plateau/Third Pole Environment Data Center (NTP/TPEDC; <https://data.tpdc.ac.cn/en/disallow/789e838e-16ac-4539-bb7e-906217305a1d>) (Zhao et al., 2017). The dataset comprised five different ground surface covers and three-four permafrost zones, spanned variable time periods during 1997–2023, and exhibited a wide range of MAPT and ALT from  $\sim -19$  °C to  $\sim 0$  °C and  $\sim 40$  cm to ~~300~~310 cm, respectively (Table C1).

170 Ground temperature data were first checked for quality and then daily means were calculated for all available depths before further processing. Thawing and freezing indices were calculated as annual sums of positive and negative mean daily ground temperatures, respectively, which were expressed in absolute values for convenience. Following standard procedures and monitoring guidelines (Streletskiy et al., 2022), ALT was determined as the maximum annual depth of the 0 °C isotherm that was tracked by linear interpolation of mean daily ground temperatures within the measured profile. MAPT was calculated  
175 as the mean annual ground temperature, which was linearly interpolated to the depth that corresponds to ALT (e.g., Hrbáček et al., 2020, 2021; Kňázková and Hrbáček, 2024). It is important to note that there is no universal method for interpolating between ground temperature sensors that works best, and therefore we used the linear interpolation, which is generally accepted (e.g., Streletskiy et al., 2022). Hereafter, these values are referred to as the observed MAPT and ALT. They were considered suitable for the evaluation because  $\sim 65$  % of the observed MAPT differed by less than 0.1 °C from the temperature of the  
180 closest temperature sensor used for the interpolation and  $\sim 80$  % of the observed ALT were less than 10 cm from the closest temperature sensor, which sets their maximum possible deviations from the actual MAPT and ALT values (Fig. 1).

Subsequently, MAPT and ALT were also modelled using ASMs given by Eq. (8) and (27) forced by the measured thawing and freezing indices from the depth intervals of 0–10 cm, 25–35 cm and 45–55 cm, which were combined into three pairs of 5/30 cm, 5/50 cm and 30/50 cm so that they were comparable across the validation sites. This provided us with three sets  
185 of MAPT and ALT estimates that allowed to determine which depth combinations worked best. The three depth pairs were situated within the active layer in all instances, and therefore differed from the temperature sensors used to determine the observed MAPT and ALT, so this did not invalidate the evaluation.

We compared the modelled MAPT and ALT directly with the observed MAPT and ALT, and evaluated the model accuracy for each site using common error metrics, such as mean error (ME), mean percentage error (MPE), mean absolute error (MAE),  
190 mean absolute percentage error (MAPE), and root-mean-square error (RMSE). The evaluation statistics were grouped by depth

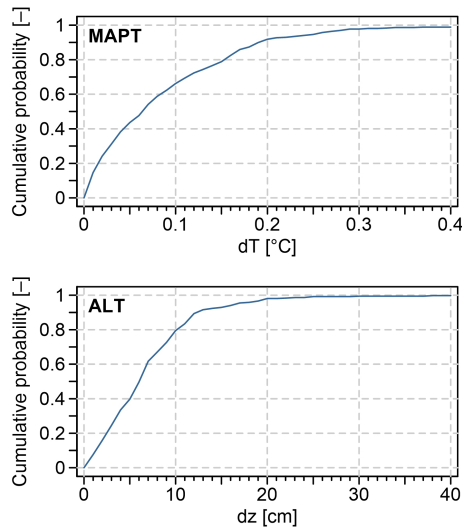


**Figure 1.** Cumulative distribution functions of the temperature differences of the observed MAPT and of the distances of the observed ALT from the closest temperature sensors used for the linear interpolation, which sets their maximum possible deviations from the actual MAPT and ALT values.

pairs and surface cover, as the latter also broadly captures the common characteristics of the validation sites in terms of climate and composition of the active layer.

## 4 Results

### 4.1 Mean annual permafrost table temperature

195 The MAPT modelled using ASM given by Eq. (8) based on the measured thawing and freezing indices for the depth pairs of 5/30 cm, 5/50 cm and 30/50 cm showed the total site-weighted ME from 0.01 °C to 0.05 °C compared to the observed MAPT (Table 1). Since the errors were scattered around zero (Fig. 42), the total site-weighted MAE was somewhat larger and ranged from 0.11 °C to 0.16 °C, while the total site-weighted RMSE was 0.12 °C to 0.19 °C (Table 1). The majority of errors were well within  $\pm 0.2$  °C (Fig. 42).

200 The accuracy of the modelled MAPT was similar for the three depth pairs, although 5/50 cm and 30/50 cm performed slightly better than 5/30 cm (Table 1). Similarly, there were rather small differences between individual surface covers (Fig. 42) that exhibited the site-weighted ME from  $-0.06$  °C to 0.12 °C (Table 1). However, the MAPT estimates were somewhat better at the vegetated sites, as the site-weighted MAE and RMSE there were mostly less than  $\sim 0.15$  °C, while the bedrock and bare-ground sites mostly showed the site-weighted MAE and RMSE greater than  $\sim 0.15$  °C (Table 1). The site-weighted errors also tended  
 205 to be somewhat larger at higher MAPT for all three depth pairs.



**Table 1.** Evaluation statistics of MAPT modelled using ASM given by Eq. (8) based on the measured thawing and freezing indices for the depth pairs of 5/30 cm, 5/50 cm and 30/50 cm and diverse surface covers.

Depth pair	Surface cover	Sites	MAPT <sub>obs</sub> [°C]	MAPT <sub>mod</sub> [°C]	ME [°C]	MAE [°C]	RMSE [°C]
5/30 cm	Bedrock	2	-1.58	-1.59	-0.01	0.07	0.10
	Bare	14	-8.84	-8.81	0.03	0.22	0.26
	Grass	10	-5.80	-5.78	0.02	0.15	0.19
	Shrub	<u>6-7</u>	<u>-2.12-2.66</u>	<u>-2.14-2.67</u>	<u>-0.02-0.00</u>	<u>0.06-0.07</u>	<u>0.06-0.07</u>
	Forest	<u>5-6</u>	<u>-0.53-1.06</u>	<u>-0.54-1.09</u>	<u>-0.01-0.03</u>	<u>0.19-0.18</u>	<u>0.21-0.20</u>
	Total	<u>37-39</u>	<u>-5.41-5.38</u>	<u>-5.40-5.37</u>	0.01	0.16	0.19
5/50 cm	Bedrock	2	<u>-1.57-1.58</u>	-1.59	-0.02	0.16	0.18
	Bare	14	<u>-8.84-8.83</u>	-8.77	0.07	0.13	0.15
	Grass	12	-4.50	-4.56	-0.06	0.12	0.14
	Shrub	<u>6-7</u>	<u>-2.12-2.66</u>	<u>-2.12-2.67</u>	<u>0.00-0.01</u>	0.04	0.04
	Forest	<u>5-13</u>	<u>-0.52-1.09</u>	<u>-0.55-1.07</u>	<u>-0.03-0.02</u>	<u>0.08-0.13</u>	<u>0.09-0.15</u>
	Total	<u>39-48</u>	<u>-5.03-4.45</u>	<u>-5.03-4.44</u>	<u>0.00-0.01</u>	<u>0.11-0.12</u>	<u>0.13</u>
30/50 cm	Bedrock	4	<u>-2.88-2.89</u>	-2.76	0.12	0.23	0.25
	Bare	14	-8.83	-8.74	0.09	0.14	0.17
	Grass	10	-5.35	-5.33	0.02	0.07	0.09
	Shrub	<u>6-7</u>	<u>-2.12-2.66</u>	<u>-2.12-2.67</u>	<u>0.00-0.01</u>	0.04	0.04
	Forest	<u>5-9</u>	<u>-0.52-1.28</u>	<u>-0.53-1.24</u>	<u>-0.01-0.04</u>	<u>0.07-0.09</u>	<u>0.08-0.10</u>
	Total	<u>39-44</u>	<u>-5.23-4.97</u>	<u>-5.18-4.92</u>	0.05	0.11	0.12

## 4.2 Active-layer thickness

The ALT modelled using ASM given by Eq. (27) based on the measured thawing indices for the depth pairs of 5/30 cm, 5/50 cm and 30/50 cm exhibited the total site-weighted ME from -7.511.5 cm (-8.39.3 %) to 0.1-1.6 cm (-0.31.2 %) compared to the observed ALT (Table 2). The total site-weighted MAE was larger (Fig. 23) and reached 12.113.1 cm (9.710.2 %) to 16.817.1 cm (19.319.8 %), while the total site-weighted RMSE was 13.214.2 cm to 18.018.2 cm (Table 2).

The accuracy of the modelled ALT was higher for the depth pairs of 5/50 cm and 30/50 cm compared to 5/30 cm, especially at the bedrock, shrub and forest sites (Table 2). Additionally, there were rather large differences between individual surface covers (Fig. 23), among which the site-weighted ME ranged from -38.133.4 cm (-34.631.3 %) to 38.0 cm (33.8 %) (Table 2). The most accurate ALT estimates were at the bare-ground sites and those with grass and shrub cover, as their site-weighted MAE ranged from 3.83.9 cm (6.0 %) to 20.122.0 cm (31.032.6 %), and the site-weighted RMSE was from 3.84.0 cm to 20.322.2 cm (Table 2). Somewhat worse was the model performance at the bedrock and forest sites, with the site-weighted MAE from

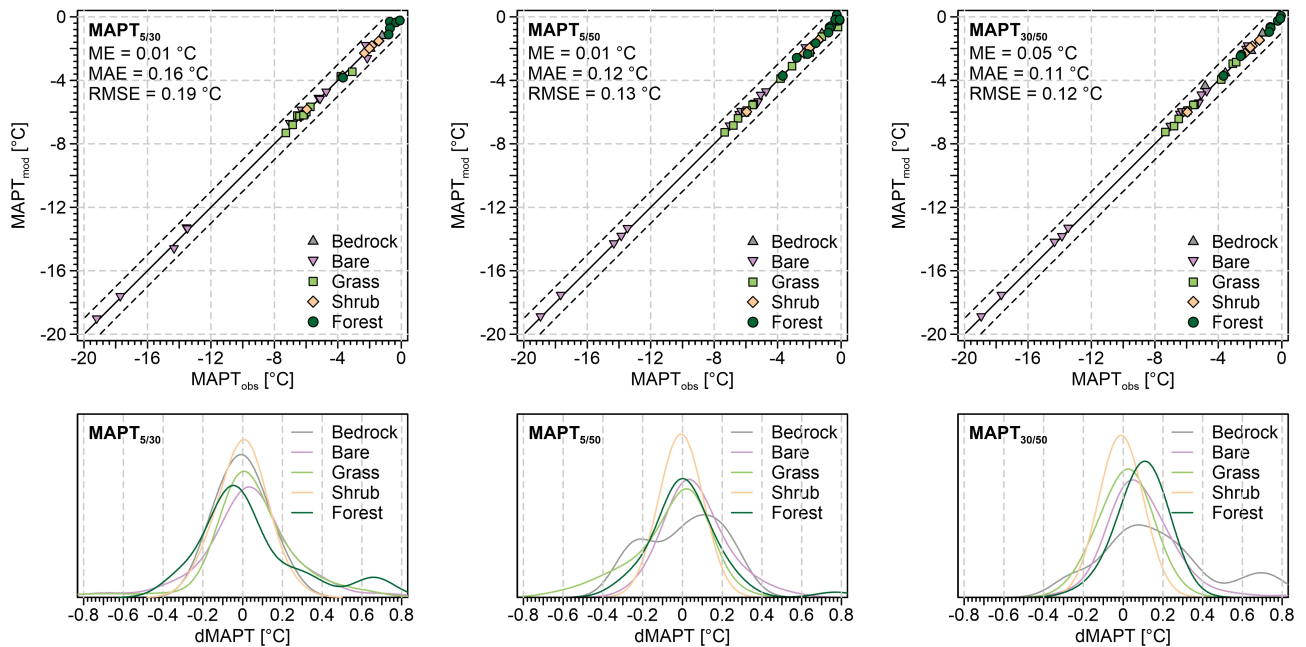


**Figure 2.** Comparison of the observed MAPT and MAPT modelled using ASM given by Eq. (8) based on the measured thawing and freezing indices for the depth pairs of 5/30 cm, 5/50 cm and 30/50 cm and diverse surface covers. The black solid and dashed lines in the upper plots represent the line of identity and the deviation of  $\pm 1$  °C, respectively.

9.0 cm (7.9 %) to ~~38.1~~38.0 cm (~~34.6~~33.8 %) and the site-weighted RMSE from 10.4 cm to 43.4 cm (Table 2). The site-weighted errors were also larger at thicker ALT for all three depth pairs.

## 5 Discussion

### 220 5.1 Mean annual permafrost table temperature

The modelled MAPT showed a relatively high accuracy for all three depth pairs and surface covers (Fig. 42), with the mean errors close to zero and the majority of them within  $\pm 0.2$  °C (Table 1), which is similar or better than in most previous studies that used other analytical or statistical models for MAPT (e.g., Romanovsky and Osterkamp, 1995; Sazonova and Romanovsky, 2003; Ferreira et al., 2017; Way and Lewkowicz, 2018; Wang et al., 2020; Kaplan Pastřriková et al., 2023).

225 Somewhat larger errors in the modelled MAPT arose especially under warmer conditions and within a thicker active layer where MAPT needs to be extrapolated to greater depth. Warmer climates are also dominated by vegetated sites (Table C1) with well-developed soils and therefore a more heterogeneous active layer where MAPT estimates are more difficult. In addition, it may also be associated with increased complexity of the system at permafrost temperatures approaching 0 °C when simple models tend to fail to a greater extent (Riseborough, 2007). The worst MAPT estimates at the bedrock sites were also likely

**Table 2.** Evaluation statistics of ALT modelled using ASM given by Eq. (27) based on the measured thawing and freezing indices for the depth pairs of 5/30 cm, 5/50 cm and 30/50 cm and diverse surface covers.

Depth pair	Surface cover	Sites	ALT <sub>obs</sub> [cm]	ALT <sub>mod</sub> [cm]	ME [cm]	MPE [%]	MAE [cm]	MAPE [%]	RMSE [cm]
5/30 cm	Bedrock	2	116.8	154.8	38.0	33.8	38.0	33.8	43.4
	Bare	14	85.1	89.1	4.0	4.3	11.3	12.0	12.9
	Grass	10	62.1	58.2	-3.9	-7.8	7.6	12.0	8.5
	Shrub	<u>6-7</u>	<u>64.3-66.4</u>	<u>44.2-54.0</u>	<u>-20.1-12.4</u>	<u>-31.0-20.5</u>	<u>20.1-22.0</u>	<u>31.0-32.6</u>	<u>20.3-22.2</u>
	Forest	<u>5-6</u>	<u>89.3-85.6</u>	<u>51.2-52.2</u>	<u>-38.1-33.4</u>	<u>-34.6-31.3</u>	<u>38.1-33.4</u>	<u>34.6-31.3</u>	<u>38.4-33.7</u>
	Total	<u>37-39</u>	<u>77.8-77.5</u>	<u>71.9-72.5</u>	<u>-5.9-5.0</u>	<u>-8.3-7.2</u>	<u>16.8-17.1</u>	<u>19.3-19.8</u>	<u>18.0-18.2</u>
5/50 cm	Bedrock	2	116.8	119.4	2.6	2.0	9.0	7.9	10.4
	Bare	14	86.3	90.7	4.4	2.4	9.1	7.6	10.3
	Grass	12	103.2	87.4	-15.8	-10.1	18.6	12.9	19.0
	Shrub	<u>6-7</u>	<u>64.3-66.5</u>	<u>57.7-62.4</u>	<u>-6.6-4.1</u>	<u>-10.3-6.8</u>	<u>6.6-7.3</u>	<u>10.3-10.9</u>	<u>6.8-7.4</u>
	Forest	<u>5-13</u>	<u>89.4-101.8</u>	<u>63.8-71.2</u>	<u>-25.6-30.6</u>	<u>-17.7-24.5</u>	<u>25.7-30.6</u>	<u>17.8-24.5</u>	<u>26.0-30.9</u>
	Total	<u>39-48</u>	<u>90.1-93.1</u>	<u>82.6-81.6</u>	<u>-7.5-11.5</u>	<u>-6.0-9.3</u>	<u>13.8-17.0</u>	<u>11.0-14.0</u>	<u>14.4-17.6</u>
30/50 cm	Bedrock	4	184.8	176.7	-8.1	-1.4	27.9	14.5	32.2
	Bare	14	86.4	93.2	6.8	3.7	11.4	9.2	12.8
	Grass	10	76.5	80.1	3.6	1.0	8.7	9.4	9.2
	Shrub	<u>6-7</u>	<u>64.3-66.4</u>	<u>62.8-65.8</u>	<u>-1.5-0.6</u>	<u>-2.5-1.3</u>	<u>3.8-3.9</u>	6.0	<u>3.8-4.0</u>
	Forest	<u>5-9</u>	<u>89.4-103.2</u>	<u>72.2-84.6</u>	<u>-17.2-18.6</u>	<u>-10.8-11.1</u>	<u>18.1-21.3</u>	<u>12.1-13.9</u>	<u>18.3-21.7</u>
	Total	<u>39-44</u>	<u>90.9-93.3</u>	<u>91.0-91.7</u>	<u>0.1-1.6</u>	<u>-0.3-1.2</u>	<u>12.1-13.1</u>	<u>9.7-10.2</u>	<u>13.2-14.2</u>

230 because active layer is thick there (Table 1). Moreover, the boreholes were drilled into vertical rockwalls, and therefore it is possible that lateral flows of heat and moisture occur in the fractured bedrock, which further complicates MAPT estimates.

So far, models for estimating MAPT have typically assumed that the ratio of thawed and frozen thermal conductivity is less than or equal to 1, and that the thermal offset is therefore negative (e.g., Gislén et al., 2013; Obu et al., 2019, 2020), which would result in invalid MAPT estimates if the actual conditions were reversed. However, although nearly half of the bedrock  
235 and bare-ground sites exhibited a positive thermal offset with a thermal conductivity ratio above 1, the MAPT was modelled with similar accuracy at these locations as elsewhere (Table 1, Fig. 12). This is because ASM utilizes measured thawing and freezing indices within the active layer and can therefore easily capture this behaviour. This is also demonstrated by the thermal conductivity ratios modelled using Eq. (5) for the three depth levels that are close to those for the whole active layer (Fig. 34), which is likely because the relationship between the thawing and freezing indices within the active layer is linear (see Sect. 2.1)  
240 and its slope varies rather slightly with vertical changes in ground physical properties.

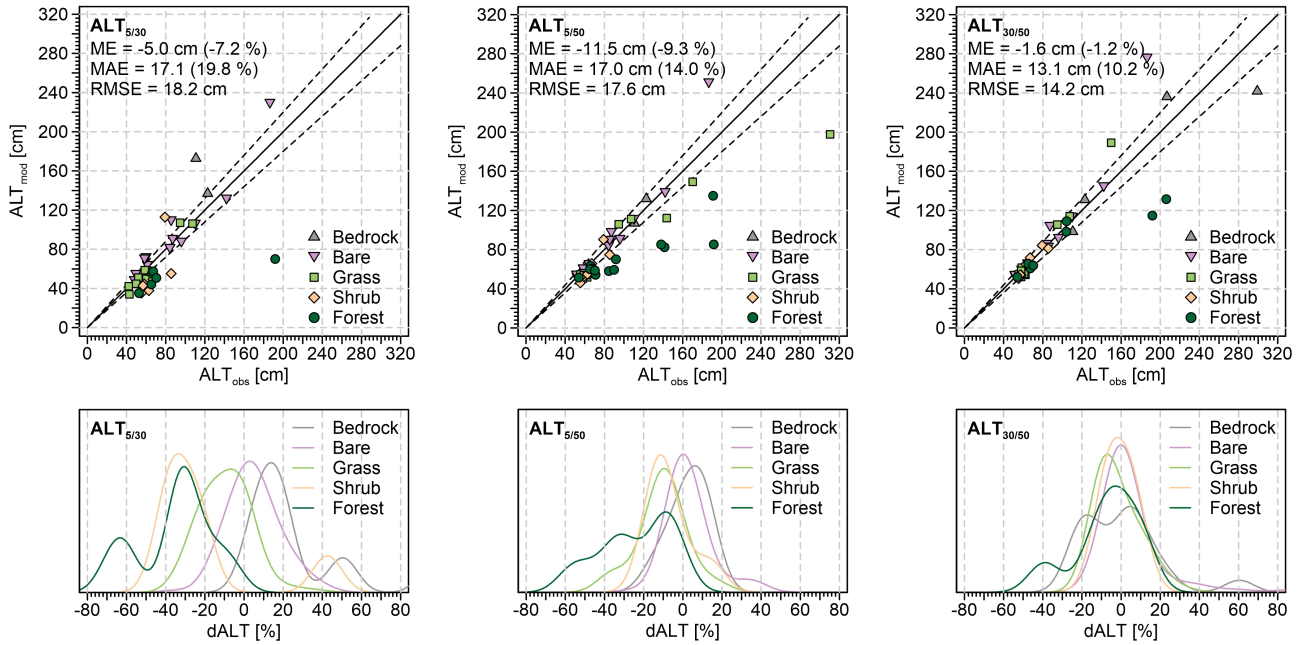


**Figure 3.** Comparison of the observed ALT and ALT modelled using ASM given by Eq. (27) based on the measured thawing and freezing indices for the depth pairs of 5/30 cm, 5/50 cm and 30/50 cm and diverse surface covers. The black solid and dashed lines in the upper plots represent the line of identity and the deviation of  $\pm 10\%$ , respectively.

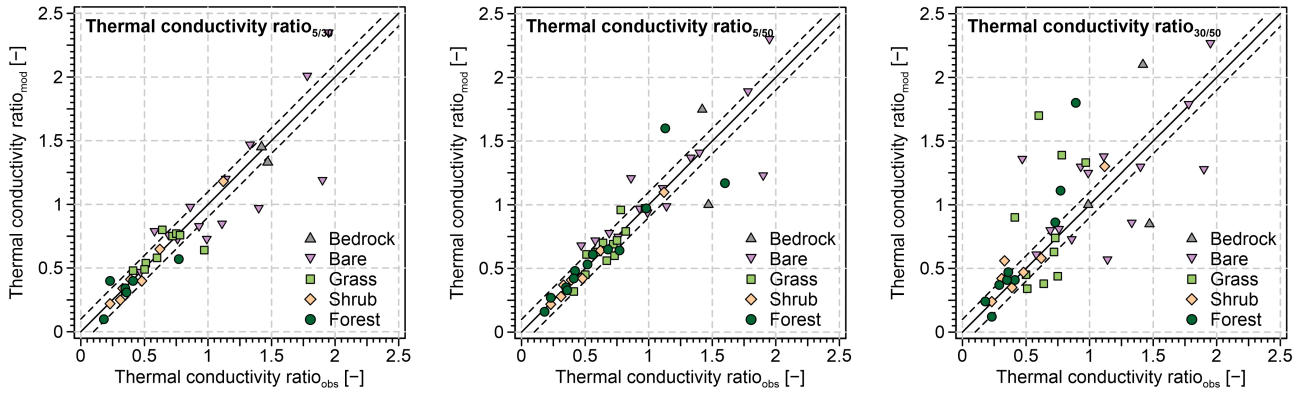


**Figure 4.** Comparison of the observed thermal conductivity ratio for the whole active layer and thermal conductivity ratio estimated using Eq. (5) based on the measured thawing and freezing indices for the depth pairs of 5/30 cm, 5/50 cm and 30/50 cm and diverse surface covers. The black solid and dashed lines represent the line of identity and the deviation of  $\pm 0.1$ .

## 5.2 Active-layer thickness

Unlike MAPT, the modelled ALT showed variable performance for individual depth pairs and surface covers (Fig. 23, Table 2). However, the errors were mostly well within  $\pm 20\%$ , which is also similar or better than in most previous studies that used other analytical or statistical models for ALT (Anisimov et al., 1997; Nelson et al., 1997; Romanovsky and Osterkamp, 1997; 245 Anisimov et al., 2002; Shiklomanov and Nelson, 2002; Sazonova and Romanovsky, 2003; Streletskiy et al., 2012; Yin et al., 2016; Zorigt et al., 2016; Hrbáček and Uxa, 2020; Kaplan Pastříková et al., 2023).

Notably, the modelled ALT showed variable accuracy for the depth pair of 5/30 cm (Table 2). This is because the active layer is typically more heterogeneous at the vegetated sites and may often comprise a surface organic layer there, the physical properties of which strongly differ from the ground underneath. This alters the temperature gradient within the active layer and 250 results in worse ALT estimates, which can be observed especially at the shrub and forest sites (Fig. 23). By contrast, the ALT estimates showed substantially lower errors for the depth pairs of 5/50 cm and 30/50 cm (Fig. 23), which largely to completely eliminated the influence of the surface layer. This also explains the consistently high accuracy of the modelled ALT at the bare-ground sites for all three depth pairs (Table 2), as the active layer there is relatively homogeneous in terms of its stratigraphy and physical properties. The ALT estimates were also relatively accurate at the bedrock sites (Table 2), but the same concern 255 exists for them as for MAPT (see Sect. 5.1). Similarly to MAPT, the modelled ALT tended to be less accurate under warmer conditions dominated by vegetated sites with a more heterogeneous and thick active layer (Table C1) where ALT needs to be extrapolated to greater depth.

Previous studies have estimated the edaphic term based on the relationship between ALT and thawing index (Nelson and Outcalt, 1987; Hinkel and Nicholas, 1995; Nelson et al., 1997; Anisimov et al., 2002; Shiklomanov and Nelson, 2002; Smith 260 et al., 2009; Shiklomanov et al., 2010; Peng et al., 2023), which is restrictive, as it requires ALT. However, the edaphic term modelled using Eq. (20) for the three depth levels was close to the edaphic term calculated for the whole active layer (Fig. 45). As with MAPT, this is because the square root of the thawing index within the active layer is linear (see Sect. 2.2) and its slope varies rather slightly with vertical changes in ground physical properties (Riseborough, 2003).

## 5.3 Model advantages

265 Unlike other analytical or statistical models for MAPT (e.g., Garagulya, 1990; Romanovsky and Osterkamp, 1995; Smith and Riseborough, 1996) and ALT (e.g., Neumann, c. 1860; Stefan, 1891; Kudryavtsev et al., 1977), ASMs given by Eq. (8) and (27) can work in any grounds where conductive heat transfer prevails without knowing their physical properties.

Although ASMs utilize only thawing and freezing indices from two depth levels within the active layer as inputs, they inherently account for the natural variability of ground physical properties in the intermediate layer between these two depths 270 [that is expressed in terms of annual and seasonal means of the thermal conductivity ratio and edaphic term, respectively.](#) Similarly, ASMs consider latent and sensible heat or other factors there, although these are not explicitly accounted for. This is because the relative values of the thawing and freezing indices at the two depth levels reflect the rate of heat transfer in the intermediate layer between them (see Eq. 5 and 20) that is influenced by seasonal changes in ground physical properties. So

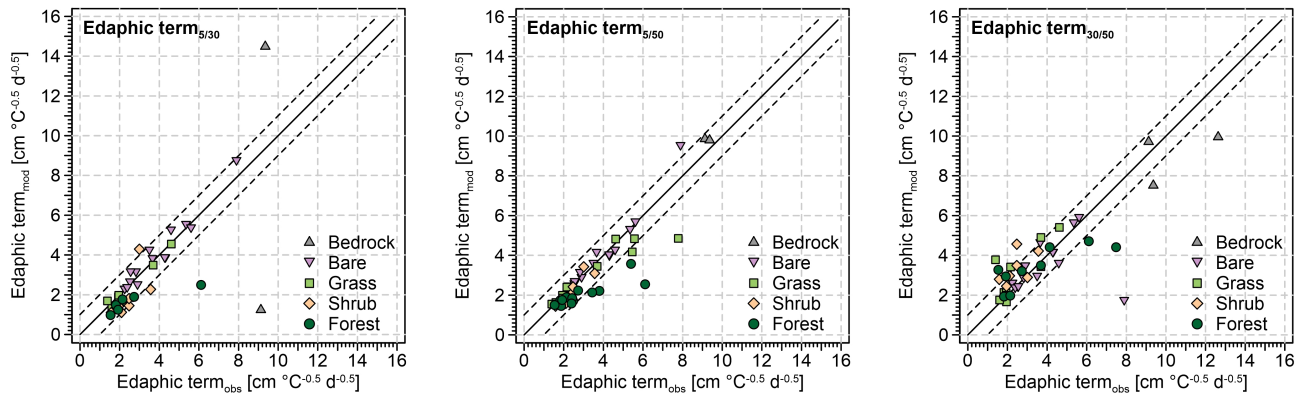


**Figure 5.** Comparison of the observed edaphic term for the whole active layer and edaphic term estimated using Eq. (20) based on the measured thawing and freezing indices for the depth pairs of 5/30 cm, 5/50 cm and 30/50 cm and diverse surface covers. The black solid and dashed lines represent the line of identity and the deviation of  $\pm 1 \text{ cm } ^\circ\text{C d}^{-0.5}$ .

in principle it is analogous to, for instance, the calculations of apparent thermal diffusivity, which are based on damping of  
 275 temperature amplitude or phase lag between two depth levels (Horton et al., 1983).

This is highly convenient because ground physical properties, such as thermal conductivity, heat capacity, water content or bulk density, are frequently unavailable or unrepresentative. Ground physical properties in other models for MAPT and ALT have therefore been estimated empirically or based on published values with unknown validity (e.g., Hinkel and Nicholas, 1995; Nelson et al., 1997; Anisimov et al., 2002; Shiklomanov and Nelson, 2002; Gislén et al., 2013; Obu et al., 2019, 2020; 280 Garibaldi et al., 2021). Ground physical properties also show more or less variability on seasonal and annual time scales (e.g., Gao et al., 2020; Hrbáček et al., 2023a; Li et al., 2023; Kňázková and Hrbáček, 2024; Wenhao et al., 2024), which most other models cannot handle because they typically treat ground physical properties as constants for whole modelling periods. Of course, ASMs ~~in-principle~~ also treat them as constants, but their values are annual or seasonal means that reflect the variations in ground physical properties over time mainly due to changes in water content and as such they are representative for individual 285 years (Eq. 8) or thawing seasons (Eq. 27), ~~which~~. This is a major improvement over other analytical or statistical models for MAPT (e.g., Garagulya, 1990; Romanovsky and Osterkamp, 1995; Smith and Riseborough, 1996) and ALT (e.g., Neumann, c. 1860; Stefan, 1891; Kudryavtsev et al., 1977).

Therefore, we believe that in addition to MAPT and ALT estimates, ASMs could also be useful for investigating temporal and spatial variations in the thermal conductivity ratio (Fig. 34) and edaphic term (Fig. 45), which might be investigated using 290 networks of miniature temperature loggers collecting data only in shallow parts of the active layer. This is because another advantage of ASMs is that their inputs can be any depth combinations from within the active layer. For most accurate outputs, however, we suggest using thawing and freezing indices from depth levels as close as possible to the permafrost table. For instance, this could improve ALT estimates at the bedrock sites where active layer is thick.

In addition to *in situ* ground temperature measurements, we suppose that ASMs could also be forced by diverse climate reanalyses or Earth system models, if these at least partially account for the physics of ground thawing and freezing. While these products have been widely used for permafrost applications (e.g., Cao et al., 2020; Kaplan Pastíriková et al., 2024; Liu et al., 2025), they typically provide only ground surface and shallow active-layer temperatures with ground physical properties largely unknown, which is frequently insufficient to determine MAPT and ALT directly or using conventional models. If the active layer is thick, MAPT and ALT have therefore usually been confined to the deepest ground temperature level available in these products, which can obviously be misleading (e.g., Cao et al., 2020). However, ASMs are designed so that they should be able to provide MAPT and ALT estimates even under these conditions.

Lastly, ASMs can also be easily reformulated to be used for estimating the mean annual temperature at the base of seasonally frozen ground and frost depth (see Appendix A and B).

#### 5.4 Model limitations

Since ASMs assume that active layer is vertically homogeneous, they can be biased if there are strong vertical changes in ground physical properties and/or higher ground-ice content near the base of the active layer (Riseborough, 2003). For instance, if temperature measurements are used from the topmost layer, whose physical properties differ from the rest of the active layer, ASMs may be inaccurate. Similarly, the modelled MAPT and ALT may be unreliable if only shallow temperature measurements in a thick active layer are used. This is because the estimates would be based on physical properties of a small portion of the active layer, which may be different in its deeper parts. Nevertheless, the natural variability of ground physical properties without sharp changes in their vertical distribution is unlikely to have a major influence on the MAPT and ALT estimates (see Fig. 1 and 2 and 3, Table 1 and 2).

Other downside of ASMs is that they require temperature measurements from two depth levels within the active layer, which may not be available at many sites.

## 6 Conclusions

We devised two novel analytical–statistical models (ASMs) for estimating MAPT and ALT given by Eq. (8) and (27), respectively, which are driven solely by thawing and freezing indices from two depth levels within the active layer, while no ground physical properties are required. ASMs reproduced MAPT and ALT in the Earth’s major permafrost regions with the total mean errors of less than 0.05 °C and 89%, respectively, which is very promising because it is similar or better than other analytical or statistical models. ASMs worked best in a homogeneous active layer with small vertical changes in ground physical properties and when permafrost table was close below the temperature sensors considered for MAPT and ALT estimates. By contrast, they performed worst in a heterogeneous and thick active layer when the topmost organic layer influenced the estimates.

We believe that ASMs can find useful applications under a wide range of climates, ground surface covers and ground physical conditions wherever at least two temperature measurements within the active layer are available. They are primarily intended to be used for MAPT or ALT estimates where ground temperature measurements are too shallow and MAPT or ALT

therefore cannot be determined directly, but they can also be used to establish typical values of the thermal conductivity ratio and the edaphic term for MAPT and ALT estimates in the past and in the future or for modelling their spatial variations. In addition to *in situ* measurements, they could utilize diverse climate reanalyses or Earth system models. Lastly, they can be easily reformulated for estimating the mean annual temperature at the base of seasonally frozen ground and frost depth.

### 330 Appendix A: Derivation of ASM for mean annual temperature at the base of seasonally frozen ground

Similarly to Eq. (1), the mean annual temperature at the base of seasonally frozen ground ( $MASFT > 0^\circ\text{C}$ ) is calculated as follows (Romanovsky and Osterkamp, 1995)

$$MASFT = \frac{I_{ts} - \frac{k_f}{k_t} I_{fs}}{P}. \quad (A1)$$

335 MASFT based on temperatures measured at two distinct depths in the seasonally freezing layer  $z_1$  and  $z_2$  ( $z_1 < z_2 < FD$ ) can therefore be expressed as follows

$$MASFT = \frac{I_{tz_1} - \frac{k_f}{k_t} I_{fz_1}}{P}, \quad (A2)$$

$$MASFT = \frac{I_{tz_2} - \frac{k_f}{k_t} I_{fz_2}}{P}. \quad (A3)$$

This implies that Eq. (A2) and (A3) are equivalent:

$$\frac{I_{tz_1} - \frac{k_f}{k_t} I_{fz_1}}{P} = \frac{I_{tz_2} - \frac{k_f}{k_t} I_{fz_2}}{P}. \quad (A4)$$

340 Solving Eq. (A4) for the inverse of the thermal conductivity ratio yields

$$\frac{k_f}{k_t} = \frac{I_{tz_1} - I_{tz_2}}{I_{fz_1} - I_{fz_2}}. \quad (A5)$$

Equation (A5) can be then substituted for the thermal conductivity ratio in Eq. (A2) and (A3) as follows

$$MASFT = \frac{I_{tz_1} - \frac{I_{tz_1} - I_{tz_2}}{I_{fz_1} - I_{fz_2}} I_{fz_1}}{P}, \quad (A6)$$

$$MASFT = \frac{I_{tz_2} - \frac{I_{tz_1} - I_{tz_2}}{I_{fz_1} - I_{fz_2}} I_{fz_2}}{P}. \quad (A7)$$

345 Subsequently, Eq. (A6) and (A7) both simplify to the same formula for MASFT:

$$MASFT = \frac{I_{fz_1} I_{tz_2} - I_{fz_2} I_{tz_1}}{P}, \quad (A8)$$

which only slightly differs from Eq. (A8).



## Appendix B: Derivation of ASM for frost depth

Similarly to Eq. (13), the frost depth (FD) can be calculated using the Stefan (1891) model as follows

$$350 \quad \text{FD} = \sqrt{\frac{2k_f I_{fs}}{L\phi}}. \quad (\text{B1})$$

As with Eq. (13), note that the freezing index must be multiplied by the scaling factor of  $86\,400 \text{ s d}^{-1}$ . FD estimated using freezing indices measured at two distinct depths  $z_1$  and  $z_2$  ( $z_1 < z_2 < \text{FD}$ ) can be expressed as follows

$$\text{FD} = z_1 + \sqrt{\frac{2k_f I_{fz_1}}{L\phi}}, \quad (\text{B2})$$

$$\text{FD} = z_2 + \sqrt{\frac{2k_f I_{fz_2}}{L\phi}}. \quad (\text{B3})$$

355 This implies that Eq. (B2) and (B3) are equivalent:

$$z_1 + \sqrt{\frac{2k_f I_{fz_1}}{L\phi}} = z_2 + \sqrt{\frac{2k_f I_{fz_2}}{L\phi}}. \quad (\text{B4})$$

The vertical distance between  $z_2$  and  $z_1$  can be expressed as

$$z_2 - z_1 = \sqrt{\frac{2k_f I_{fz_1}}{L\phi}} - \sqrt{\frac{2k_f I_{fz_2}}{L\phi}}, \quad (\text{B5})$$

which simplifies to

$$360 \quad z_2 - z_1 = \sqrt{\frac{2k_f}{L\phi}} \left( \sqrt{I_{fz_1}} - \sqrt{I_{fz_2}} \right). \quad (\text{B6})$$

Subsequently rearranging Eq. (B6) gives

$$\frac{z_2 - z_1}{\sqrt{I_{fz_1}} - \sqrt{I_{fz_2}}} = \sqrt{\frac{2k_f}{L\phi}}, \quad (\text{B7})$$

where the right-hand side corresponds to the edaphic term, which combines the ground physical properties in the Stefan model into a single variable. The edaphic term can be implemented in Eq. (B2) and (B3) as

$$365 \quad \text{FD} = z_1 + E \sqrt{I_{fz_1}}, \quad (\text{B8})$$

$$\text{FD} = z_2 + E \sqrt{I_{fz_2}}. \quad (\text{B9})$$

Substituting the left-hand side of Eq. (B7) for the edaphic term in Eq. (B8) and (B9) yields

$$\text{FD} = z_1 + \frac{z_2 - z_1}{\sqrt{I_{fz_1}} - \sqrt{I_{fz_2}}} \sqrt{I_{fz_1}}, \quad (\text{B10})$$

$$\text{FD} = z_2 + \frac{z_2 - z_1}{\sqrt{I_{fz_1}} - \sqrt{I_{fz_2}}} \sqrt{I_{fz_2}}. \quad (\text{B11})$$

370 Simplifying Eq. (B10) and (B11) then produces the same formula for FD:

$$\text{FD} = \frac{z_2 \sqrt{I_{fz_1}} - z_1 \sqrt{I_{fz_2}}}{\sqrt{I_{fz_1}} - \sqrt{I_{fz_2}}}, \quad (\text{B12})$$

which is the same as Eq. (27), but with the freezing indices instead of the thawing ones.

## Appendix C

Hoher Sonnblick 1	European Alps	47.05403	12.95752	3105	Bedrock	Mountain	2008–2011	4	-1.21	122.8	GTN-P
Hoher Sonnblick 3	European Alps	47.05351	12.95760	3079	Bedrock	Mountain	2016–2018	3	-1.95	110.7	GTN-P
Abernethy Flats	James Ross Island	-63.88138	-57.94832	41	Bare	Continuous	2014–2019	6	-6.36	62.5	MU
Berry Hill slopes	James Ross Island	-63.80267	-57.83863	56	Bare	Continuous	2018–2020	3	-5.24	84.2	MU
CALM	James Ross Island	-63.80190	-57.88460	10	Bare	Continuous	2015–2023	7	-4.74	87.1	MU
Johann Gregor Mendel	James Ross Island	-63.80152	-57.88330	10	Bare	Continuous	2012–2023	12	-5.13	61.3	MU
Johnson Mesa	James Ross Island	-63.82250	-57.93280	340	Bare	Continuous	2013–2023	11	-6.32	60.0	MU
Bull Pass	McMurdo Sound	-77.51847	161.86269	141	Bare	Continuous	2000–2022	22	-19.20	47.9	USDA
Granite Harbour	McMurdo Sound	-77.00655	162.52561	6	Bare	Continuous	2008–2015	4	-14.33	85.7	USDA
Marble Point	McMurdo Sound	-77.41955	163.68247	47	Bare	Continuous	2000–2022	20	-17.71	49.6	USDA
Endalen	Svalbard	78.19021	15.78158	40	Bare	Continuous	2009–2015	5	-2.25	142.1	GTN-P
Kapp Linne 2	Svalbard	78.05461	13.63667	21	Bare	Continuous	2009–2017	7	-2.15	186.5	GTN-P
Mould Bay 1	Prince Patrick Island	76.22869	-119.29893	36	Bare	Continuous	2008–2011	4	-13.53	59.7	GTN-P
Mould Bay 2	Prince Patrick Island	76.22869	-119.29893	36	Bare	Continuous	2008–2012	5	-13.47	58.4	GTN-P
Villum 1	Greenland	81.57928	-16.64330	36	Bare	Continuous	2015–2020	6	-7.03	96.1	GTN-P
Villum 2	Greenland	81.57958	-16.64752	27	Bare	Continuous	2015–2020	5	-6.30	110.2	GTN-P
Alqasuk	Alaska	70.45242	-157.41178	22	Grass	Continuous	2001–2010	9	-5.74	55.7	USDA
Barrow (site 1)	Alaska	71.32242	-156.61089	9	Grass	Continuous	1997–2017	16	-7.28	56.6	USDA
Betty Pingo; polygon center	Alaska	70.28258	-148.89347	12	Grass	Continuous	2006–2022	9	-6.12	42.3	USDA
Betty Pingo; polygon rim	Alaska	70.28258	-148.89347	12	Grass	Continuous	2006–2012	7	-5.98	52.1	USDA
Westdoock (high); polygon center	Alaska	70.37039	-148.56867	3	Grass	Continuous	2004–2020	17	-6.56	58.5	USDA
Westdoock (high); polygon rim	Alaska	70.37039	-148.56867	3	Grass	Continuous	2004–2020	17	-6.85	60.2	USDA
Westdoock (high); polygon trough	Alaska	70.37039	-148.56867	3	Grass	Continuous	2004–2020	14	-6.42	49.9	USDA
Westdoock (low); polygon trough	Alaska	70.37047	-148.56561	2	Grass	Continuous	2008–2022	9	-6.17	43.0	USDA
Old Auroral Station	Alaska	78.20146	15.83465	8	Grass	Continuous	2009–2015	7	-3.81	94.8	GTN-P
Petuniabukta	Svalbard	78.70306	16.46778	15	Grass	Continuous	2012–2018	7	-3.09	107.5	MU
QT01	Qinghai-Tibetan Plateau	35.14000	93.04000	4710	Grass	Discontinuous	2004–2013	10	-1.97	170.2	NTP/TPEDC
QT05	Qinghai-Tibetan Plateau	33.96000	92.34000	4620	Grass	Discontinuous	2004–2013	10	-0.20	310.7	NTP/TPEDC
QT09	Qinghai-Tibetan Plateau	35.72000	94.13000	4450	Grass	Discontinuous	2011–2018	8	-1.21	143.6	NTP/TPEDC
TSHAL	Qinghai-Tibetan Plateau	35.36000	79.55000	4850	Grass	Discontinuous	2016–2018	3	-2.87	149.8	NTP/TPEDC
Ivotuk 3	Alaska	68.47890	-155.73809	565	Shrub	Continuous	2011–2012	2	-2.33	57.8	GTN-P
Ivotuk 3–2	Alaska	68.47890	-155.73809	565	Shrub	Continuous	2011–2012	2	-1.84	55.4	GTN-P
Kuguruk Cabin	Alaska	66.56238	-159.00464	7	Shrub	Continuous	2013–2013	1	-3.70	56.9	GI-UAF
Kuparuk Basin 03	Alaska	68.63490	-149.36393	820	Shrub	Continuous	2016–2017	2	-2.00	62.9	GI-UAF
Kuparuk Basin 1391	Alaska	68.64262	-149.38097	782	Shrub	Continuous	2016–2017	2	-1.41	85.6	GI-UAF
Kuparuk Basin 31	Alaska	68.63294	-149.36136	822	Shrub	Continuous	2016–2017	2	-1.42	67.1	GI-UAF
<a href="#">Kuglukuk F5</a>	<a href="#">Nunavut</a>	<a href="#">67.77220</a>	<a href="#">-115.26770</a>	<a href="#">5</a>	<a href="#">Shrub</a>	<a href="#">Continuous</a>	<a href="#">2021–2022</a>	<a href="#">2</a>	<a href="#">-5.94</a>	<a href="#">79.3</a>	<a href="#">ND</a>
Bontanza Creek 1	Alaska	64.70694	-148.29128	125	Forest	Discontinuous	2012–2016	5	-0.73	65.9	GI-UAF
<a href="#">College Pent</a>	<a href="#">Alaska</a>	<a href="#">64.86781</a>	<a href="#">-147.78486</a>	<a href="#">137</a>	<a href="#">Forest</a>	<a href="#">Discontinuous</a>	<a href="#">2008–2008</a>	<a href="#">1</a>	<a href="#">-3.69</a>	<a href="#">67.3</a>	<a href="#">GI-UAF</a>
Fox	Alaska	64.95061	-147.61769	240	Forest	Discontinuous	2013–2015	3	-0.33	52.7	GI-UAF
Gakona 1	Alaska	62.39292	-145.14528	550	Forest	Continuous	2010–2014	5	-0.71	65.2	GI-UAF
Gakona 2	Alaska	62.39128	-145.14689	548	Forest	Continuous	2013–2013	1	-0.80	70.4	GI-UAF
Smith Lake	Alaska	64.86752	-147.85883	158	Forest	Discontinuous	2007–2011	5	-0.11	191.9	GTN-P
<a href="#">Beaver Creek</a>	<a href="#">Yukon</a>	<a href="#">62.33333</a>	<a href="#">-140.83333</a>	<a href="#">649</a>	<a href="#">Forest</a>	<a href="#">Discontinuous</a>	<a href="#">2009–2019</a>	<a href="#">11</a>	<a href="#">-2.55</a>	<a href="#">104.2</a>	<a href="#">ND</a>
<a href="#">Beaver Creek BH3</a>	<a href="#">Yukon</a>	<a href="#">62.38427</a>	<a href="#">-140.87044</a>	<a href="#">660</a>	<a href="#">Forest</a>	<a href="#">Discontinuous</a>	<a href="#">2023–2023</a>	<a href="#">1</a>	<a href="#">-2.12</a>	<a href="#">84.8</a>	<a href="#">YPD</a>
<a href="#">Cowley Creek 1</a>	<a href="#">Yukon</a>	<a href="#">60.59306</a>	<a href="#">-134.90500</a>	<a href="#">712</a>	<a href="#">Forest</a>	<a href="#">Sporadic</a>	<a href="#">2009–2011</a>	<a href="#">3</a>	<a href="#">-0.27</a>	<a href="#">191.1</a>	<a href="#">YPD</a>
<a href="#">Cowley Creek 2</a>	<a href="#">Yukon</a>	<a href="#">60.59303</a>	<a href="#">-134.90454</a>	<a href="#">718</a>	<a href="#">Forest</a>	<a href="#">Sporadic</a>	<a href="#">2019–2023</a>	<a href="#">3</a>	<a href="#">-0.10</a>	<a href="#">141.5</a>	<a href="#">YPD</a>
<a href="#">Deuson Dump</a>	<a href="#">Yukon</a>	<a href="#">64.03186</a>	<a href="#">-139.29470</a>	<a href="#">344</a>	<a href="#">Forest</a>	<a href="#">Discontinuous</a>	<a href="#">2010–2019</a>	<a href="#">6</a>	<a href="#">-1.60</a>	<a href="#">70.9</a>	<a href="#">YPD</a>
<a href="#">Eagle River</a>	<a href="#">Yukon</a>	<a href="#">66.44463</a>	<a href="#">-136.70894</a>	<a href="#">330</a>	<a href="#">Forest</a>	<a href="#">Continuous</a>	<a href="#">2023–2023</a>	<a href="#">1</a>	<a href="#">-2.81</a>	<a href="#">91.9</a>	<a href="#">YPD</a>
<a href="#">Faro</a>	<a href="#">Yukon</a>	<a href="#">62.22356</a>	<a href="#">-133.34202</a>	<a href="#">720</a>	<a href="#">Forest</a>	<a href="#">Discontinuous</a>	<a href="#">2009–2009</a>	<a href="#">1</a>	<a href="#">-0.62</a>	<a href="#">89.8</a>	<a href="#">YPD</a>
<a href="#">Haines Junction BH1</a>	<a href="#">Yukon</a>	<a href="#">60.81556</a>	<a href="#">-137.40167</a>	<a href="#">670</a>	<a href="#">Forest</a>	<a href="#">Sporadic</a>	<a href="#">2022–2023</a>	<a href="#">2</a>	<a href="#">-0.07</a>	<a href="#">206.0</a>	<a href="#">YPD</a>

*Data availability.* The validation data from James Ross Island and Petuniabukta are available upon request from Filip Hrbáček (hrbacek-filip@gmail.com) and Kamil Láska (laska@sci.muni.cz), respectively, while the other data are available from Global Terrestrial Network for Permafrost (<http://gtnpdatabase.org>), Natural Resources Conservation Service of the United States Department of Agriculture (<https://www.nrcs.usda.gov/resources/data-and-reports/soil-climate-research-stations>), Geophysical Institute Permafrost Laboratory of the University of Alaska Fairbanks (<https://permafrost.gi.alaska.edu>), Yukon Permafrost Database (YPD, <https://service.yukon.ca/permafrost/>), Nordica D of the Centre for Northern Studies (ND, <https://nordicana.cen.ulaval.ca/en/>), and National Tibetan Plateau/Third Pole Environment Data Center (<https://data.tpdc.ac.cn/en/disallow/789e838e-16ac-4539-bb7e-906217305a1d>).

*Author contributions.* TU: conceptualization, methodology, software, validation, formal analysis, resources, investigation, writing – original draft, visualization. FH: conceptualization, resources, writing – review & editing, supervision, funding acquisition. MK: formal analysis, resources, writing – review & editing.

*Competing interests.* The contact author has declared that none of the authors has any competing interests.

*Acknowledgements.* We thank Kamil Láska and acknowledge the Global Terrestrial Network for Permafrost, Natural Resources Conservation Service of the United States Department of Agriculture, Geophysical Institute Permafrost Laboratory of the University of Alaska Fairbanks, [Yukon Permafrost Database](#), [Centre for Northern Studies](#), and National Tibetan Plateau/Third Pole Environment Data Center for collecting long-term ground temperature data and disseminating them personally and/or publicly.

*Financial support.* The research was funded by the Czech Science Foundation (project number GM22-28659M).

390 **References**

- Aalto, J., Karjalainen, O., Hjort, J., and Luoto, M.: Statistical forecasting of current and future Circum-Arctic ground temperatures and active layer thickness, *Geophys. Res. Lett.*, 45, 4889–4898, 2018.
- Anisimov, O. A., Shiklomanov, N. I., and Nelson, F. E.: Global warming and active-layer thickness: results from transient general circulation models, *Glob. Planet. Change*, 15, 61–77, [https://doi.org/10.1016/S0921-8181\(97\)00009-X](https://doi.org/10.1016/S0921-8181(97)00009-X), 1997.
- 395 Anisimov, O. A., Shiklomanov, N. I., and Nelson, F. E.: Variability of seasonal thaw depth in permafrost regions: a stochastic modeling approach, *Ecol. Model.*, 153, 217–227, [https://doi.org/10.1016/S0304-3800\(02\)00016-9](https://doi.org/10.1016/S0304-3800(02)00016-9), 2002.
- Biskaborn, B. K., Lanckman, J.-P., Lantuit, H., Elger, K., Streletskiy, D. A., Cable, W. L., and Romanovsky, V. E.: The new database of the Global Terrestrial Network for Permafrost (GTN-P), *Earth Syst. Sci. Data*, 7, 245–259, <https://doi.org/10.5194/essd-7-245-2015>, 2015.
- Bonnaventure, P. P. and Lamoureux, S. F.: The active layer: A conceptual review of monitoring, modelling techniques and changes in a warming climate, *Prog. Phys. Geog.*, 37, 352–376, <https://doi.org/10.1177/0309133313478314>, 2013.
- 400 Brown, J., Hinkel, K. M., and Nelson, F. E.: The ~~circumpolar active layer monitoring (calm) program: Research designs and initial results~~Circumpolar Active Layer Monitoring (CALM) Program: Research Designs and Initial Results, *Polar Geogr.*, 24, 166–258, <https://doi.org/10.1080/10889370009377698>, 2000.
- Burn, C. R.: The Active Layer: Two Contrasting Definitions, *Permafrost Periglac.*, 9, 411–416, [https://doi.org/10.1002/\(SICI\)1099-1530\(199810/12\)9:4<411::AID-PPP292>3.0.CO;2-6](https://doi.org/10.1002/(SICI)1099-1530(199810/12)9:4<411::AID-PPP292>3.0.CO;2-6), 1998.
- 405 Cao, B., Gruber, S., Zheng, D., and Li, X.: The ERA5-Land soil temperature bias in permafrost regions, *The Cryosphere*, 14, 2581–2595, <https://doi.org/10.5194/tc-14-2581-2020>, 2020.
- de Pablo, M. A., Ramos, M., Molina, A., and Prieto, M.: Thaw depth spatial and temporal variability at the Limnopolar Lake CALM-S site, Byers Peninsula, Livingston Island, Antarctica, *Sci. Total Environ.*, 615, 814–827, <https://doi.org/10.1016/j.scitotenv.2017.09.284>, 2018.
- 410 Farzamian, M., Vieira, G., Monteiro Santos, F. A., Yaghoobi Tabar, B., Hauck, C., Paz, M. C., Bernardo, I., Ramos, M., and de Pablo, M. A.: Detailed detection of active layer freeze–thaw dynamics using quasi-continuous electrical resistivity tomography (Deception Island, Antarctica), *The Cryosphere*, 14, 1105–1120, <https://doi.org/10.5194/tc-14-1105-2020>, 2020.
- Ferreira, A., Vieira, G., Ramos, M., and Nieuwendam, A.: Ground temperature and permafrost distribution in Hurd Peninsula (Livingston Island, Maritime Antarctic): An assessment using freezing indexes and TTOP modelling, *Catena*, 149, 560–571, <http://dx.doi.org/10.1016/j.catena.2016.08.027>, 2017.
- 415 Gao, Z., Lin, Z., Niu, F., and Luo, J.: Soil water dynamics in the active layers under different land-cover types in the permafrost regions of the Qinghai–Tibet Plateau, China. *Geoderma*, 364, 114176, <https://doi.org/10.1016/j.geoderma.2020.114176>, 2020.
- Garagulya, L. S.: *Application of Mathematical Methods and Computers in Investigations of Geocryological Processes*, Moscow University Press, Moscow, Russia, 124 pp., 1990.
- 420 Garibaldi, M. C., Bonnaventure, P. P., and Lamoureux, S. F.: Utilizing the TTOP model to understand spatial permafrost temperature variability in a High Arctic landscape, Cape Bounty, Nunavut, Canada, *Permafrost Periglac.*, 32, 19–34, <https://doi.org/10.1002/ppp.2086>, 2021.
- Gisnås, K., Etzelmüller, B., Farbrot, H., Schuler, T. V., and Westermann, S.: CryoGRID 1.0: Permafrost Distribution in Norway estimated by a Spatial Numerical Model, *Permafrost Periglac.*, 24, 2–19, <https://doi.org/10.1002/ppp.1765>, 2013.
- 425 Grosse, G., Goetz, S., McGuire, A. D., Romanovsky, V. E., and Schuur, E. A. G.: Changing permafrost in a warming world and feedbacks to the Earth system, *Environ. Res. Lett.*, 11, 040201, <https://doi.org/10.1088/1748-9326/11/4/040201>, 2016.

- Hauck, C.: Frozen ground monitoring using DC resistivity tomography, *Geophys. Res. Lett.*, 29, 2016, <https://doi.org/10.1029/2002GL014995>, 2002.
- Hayashi, M., Goeller, N., Quinton, W. L., and Wright, N.: A simple heat-conduction method for simulating the frost-table depth in hydro-  
430 logical models, *Hydrol. Process.*, 21, 2610–2622, <https://doi.org/10.1002/hyp.6792>, 2007.
- Hinkel, K. M., Nicholas, J. R. J.: Active Layer Thaw Rate at a Boreal Forest Site in Central Alaska, U.S.A., *Arct. Alp. Res.*, 27, 72–80, <https://doi.org/10.2307/1552069>, 1995.
- Hjort, J., Streletskiy, D., Doré, G., Wu, Q., Bjella, K., and Luoto, M.: Impacts of permafrost degradation on infrastructure, *Nat. Rev. Earth Environ.*, 3, 24–38, <https://doi.org/10.1038/s43017-021-00247-8>, 2022.
- 435 Hrbáček, F. and Uxa, T.: The evolution of a near-surface ground thermal regime and modeled active-layer thickness on James Ross Island, Eastern Antarctic Peninsula, in 2006–2016, *Permafrost Periglac.*, 31, 141–155, <https://doi.org/10.1002/ppp.2018>, 2020.
- Hrbáček, F., Kňazková, M., Nývlt, D., Láska, K., Mueller, C. W., and Ondruch, J.: Active layer monitoring at CALM-S site near J. G. Mendel Station, James Ross Island, eastern Antarctic Peninsula, *Sci. Total Environ.*, 601–602, 987–997, <https://doi.org/10.1016/j.scitotenv.2017.05.266>, 2017a.
- 440 Hrbáček, F., Nývlt, D., and Láska, K.: Active layer thermal dynamics at two lithologically different sites on James Ross Island, Eastern Antarctic Peninsula, *Catena*, 149, 592–602, <https://doi.org/10.1016/j.catena.2016.06.020>, 2017b.
- Hrbáček, F., Cannone, N., Kňazková, M., Malfasi, F., Convey, P., and Guglielmin, M.: Effect of climate and moss vegetation on ground surface temperature and the active layer among different biogeographical regions in Antarctica, *Catena*, 190, 104562, <https://doi.org/10.1016/j.catena.2020.104562>, 2020.
- 445 Hrbáček, F., Engel, Z., Kňazková, M., and Smolíková, J.: Effect of summer snow cover on the active layer thermal regime and thickness on CALM-S JGM site, James Ross Island, eastern Antarctic Peninsula, *Catena*, 207, 105608, <https://doi.org/10.1016/j.catena.2021.105608>, 2021.
- Hrbáček, F., Kňazková, M., Farzamian, M., and Baptista, J.: Variability of soil moisture on three sites in the Northern Antarctic Peninsula in 2022/23, *Czech Polar Rep.*, 13, 10–23, <https://doi.org/10.5817/CPR2023-1-2>, 2023a.
- 450 Hrbáček, F., Oliva, M., Hansen, C., Balks, M., O'Neill, T. A., de Pablo, M. A., Ponti, S., Ramos, M., Vieira, G., Abramov, A., Kaplan Pastíriková, L., Guglielmin, M., Goyanes, G., Rocha Francelino, M., Schaefer, C., and Lacelle, D.: Active layer and permafrost thermal regimes in the ice-free areas of Antarctica, *Earth-Sci. Rev.*, 242, 104458, <https://doi.org/10.1016/j.earscirev.2023.104458>, 2023b.
- Hrbáček, F., Kňazková, M., Láska, K., and Kaplan Pastíriková, L.: Active Layer Warming and Thickening on CALM-S JGM, James Ross Island, in the Period 2013/14–2022/23, *Permafrost Periglac.*, <https://doi.org/10.1002/ppp.2274>, 2025.
- 455 Horton, R., Wierenga, P. J., and Nielsen, D. R.: Evaluation of Methods for Determining the Apparent Thermal Diffusivity of Soil Near the Surface, *Soil. Sci. Soc. Am. J.*, 47, 25–32, <https://doi.org/10.2136/sssaj1983.03615995004700010005x>, 1983.
- Kaplan Pastíriková, L., Hrbáček, F., Uxa, T., and Láska, K.: Permafrost table temperature and active layer thickness variability on James Ross Island, Antarctic Peninsula, in 2004–2021, *Sci. Total Environ.*, 869, 161690, <https://doi.org/10.1016/j.scitotenv.2023.161690>, 2023.
- Kaplan Pastíriková, L., Hrbáček, F., and Matějka, M.: Validation of ERA5-Land-based reconstructed air temperature and near-surface ground  
460 temperature on James Ross Island. *Polar Geogr.*, 1–21, <https://doi.org/10.1080/1088937X.2024.2434744>, 2024.
- Kňazková, M. and Hrbáček, F.: Interannual variability of soil thermal conductivity and moisture on the Abernethy Flats (James Ross Island) during thawing seasons 2015–2023, *Catena*, 234, 107640, <https://doi.org/10.1016/j.catena.2023.107640>, 2024.
- Kudryavtsev, V. A., Garagulia, L., Kondratyeva, K. A., and Melamed, V. G.: Fundamentals of Frost Forecasting in Geological Engineering Investigations, Draft Translation 606, U.S. Army Cold Regions Research And Engineering Lab, Hanover, NH, 489 pp., 1977.

- 465 Lawrence, D. M., Koven, C. D., Swenson, S. C., Riley, W. J., and Slater, A. G.: Permafrost thaw and resulting soil moisture changes regulate projected high-latitude CO<sub>2</sub> and CH<sub>4</sub> emissions, *Environ. Res. Lett.*, 10, 094011, <https://doi.org/10.1088/1748-9326/10/9/094011>, 2015.
- Li, G., Zhang, M., Pei, W., Melnikov, A., Khristoforov, I., Li, R., and Yu, F.: Changes in permafrost extent and active layer thickness in the Northern Hemisphere from 1969 to 2018, *Sci. Total Environ.*, 804, 150182, <https://doi.org/10.1016/j.scitotenv.2021.150182>, 2022.
- Li, W., Weng, B., Yan, D., Lai, Y., Li, M., and Wang, H.: Underestimated permafrost degradation: Improving the TTOP model based on soil  
470 thermal conductivity, *Sci. Total Environ.*, 854, 158564, <https://doi.org/10.1016/j.scitotenv.2022.158564>, 2023.
- Liu, Z., Guo, D., Hua, W., and Chen, Y.: Near-surface permafrost extent and active layer thickness characterized by reanalysis/assimilation data. *Atmos. Sci. Lett.*, 26, e1289. <https://doi.org/10.1002/asl.1289>, 2025.
- Lunardini, V. J.: *Heat Transfer in Cold Climates*, Van Nostrand Reinhold Co., New York, NY, 731 pp., 1981.
- Nelson, F. E. and Outcalt, S. I.: A Computational Method for Prediction and Regionalization of Permafrost, *Arctic Alpine Res.*, 19, 279–288,  
475 <https://doi.org/10.2307/1551363>, 1987.
- Nelson, F. E., Shiklomanov, N. I., Mueller, G., Hinkel, K. M., Walker, D. A., and Bockheim, J. G.: Estimating Active-Layer Thickness over a Large Region: Kuparuk River Basin, Alaska, U.S.A., *Arct. Alp. Res.*, 29, 367–378, <https://doi.org/10.2307/1551985>, 1997.
- Neumann, F.: Lectures given in the 1860's, cf. Riemann-Weber, *Die Partiellen Differentialgleichungen der Mathematischen, Physik*, 2, 117–121, c. 1860.
- 480 Noetzli, J., Arenson, L. U., Bast, A., Beutel, J., Delaloye, R., Farinotti, D., Gruber, S., Gubler, H., Haerberli, W., Hasler, A., Hauck, C., Hiller, M., Hoelzle, M., Lambiel, C., Pellet, C., Springman, S. M., Vonder Muehll, D., and Phillips, M.: Best Practice for Measuring Permafrost Temperature in Boreholes Based on the Experience in the Swiss Alps, *Front. Earth Sci.*, 9, 607875, <https://doi.org/10.3389/feart.2021.607875>, 2021.
- Noetzli, J., Christiansen, H. H., Guglielmin, M., Hrbáček, F., Hu, G., Isaksen, K., Magnin, F., Pogliotti, P., Smith, S. L., Zhao, L., and  
485 Streletskiy, D. A.: Permafrost temperature and active-layer thickness, in: State of the Climate in 2023, *Bull. Amer. Meteor. Soc.*, 105, S43–S44. <https://doi.org/10.1175/2024BAMSStateoftheClimate.1>, 2024.
- Obu, J.: How Much of the Earth's Surface is Underlain by Permafrost?, *J. Geophys. Res.–Earth*, 126, e2021JF006123, <https://doi.org/10.1029/2021JF006123>, 2021.
- Obu, J., Westermann, S., Bartsch, A., Berdnikov, N., Christiansen, H. H., Dashtseren, A., Delaloye, R., Elberling, B., Etzelmüller, B.,  
490 Kholodov, A., Khomutov, A., Kääb, A., Leibman, M. O., Lewkowicz, A. G., Panda, S. K., Romanovsky, V., Way, R. G., Westergaard-Nielsen, A., Wu, T., Yamkhin, J., and Zou, D.: Northern Hemisphere permafrost map based on TTOP modelling for 2000–2016 at 1 km<sup>2</sup> scale, *Earth Sci. Rev.*, 193, 299–316, <https://doi.org/10.1016/j.earscirev.2019.04.023>, 2019.
- Obu, J., Westermann, S., Vieira, G., Abramov, A., Balks, M. R., Bartsch, A., Hrbáček, F., Kääb, A., and Ramos, M.: Pan-Antarctic map of near-surface permafrost temperatures at 1 km<sup>2</sup> scale, *The Cryosphere*, 14, 497–519, <https://doi.org/10.5194/tc-14-497-2020>, 2020.
- 495 Peng, X., Zhang, T., Frauenfeld, O. W., Mu, C., Wang, K., Wu, X., Guo, D., Luo, J., Hjort, J., Aalto, J., Karjalainen, O., and Luoto, M.: Active Layer Thickness and Permafrost Area Projections for the 21st Century, *Earth's Future*, 11, e2023EF003573, <https://doi.org/10.1029/2023EF003573>, 2023.
- Riseborough, D.: Thawing and freezing indices in the active layer, in: *Proceedings of the 8th International Conference on Permafrost*, Zurich, Switzerland, 21–25 July 2003, 953–958, 2003.
- 500 Riseborough, D. W.: Exploring the parameters of a simple model of the permafrost-climate relationship, Ph.D. thesis, Carleton University, Ottawa, 328 pp., 2004.

- Riseborough, D.: The effect of transient conditions on an equilibrium permafrost-climate model. *Permafrost Periglac.*, 18, 21–32, <https://doi.org/10.1002/ppp.579>, 2007.
- Riseborough, D. W.: Estimating active layer and talik thickness from temperature data: implications from modeling results, in: Proceedings of the 9th International Conference on Permafrost, Fairbanks, Alaska, 29 June–3 July 2008, 1487–1492, 2008.
- 505 Riseborough, D., Shiklomanov, N., Eitzelmüller, B., Gruber, S., and Marchenko, S.: Recent advances in permafrost modelling, *Permafrost Periglac.*, 19, 137–156, <https://doi.org/10.1002/ppp.615>, 2008.
- Romanovsky, V. E. and Osterkamp, T. E.: Interannual Variations of the Thermal Regime of the Active Layer and Near-Surface Permafrost in Northern Alaska, *Permafrost Periglac.*, 6, 313–335, <https://doi.org/10.1002/ppp.3430060404>, 1995.
- 510 Romanovsky, V. E. and Osterkamp, T. E.: Thawing of the Active Layer on the Coastal Plain of the Alaskan Arctic, *Permafrost Periglac.*, 8, 1–22, [https://doi.org/10.1002/\(SICI\)1099-1530\(199701\)8:1<1::AID-PPP243>3.0.CO;2-U](https://doi.org/10.1002/(SICI)1099-1530(199701)8:1<1::AID-PPP243>3.0.CO;2-U), 1997.
- Sazonova, T. S. and Romanovsky, V. E.: A model for regional-scale estimation of temporal and spatial variability of active layer thickness and mean annual ground temperatures *Permafrost Periglac.*, 14, 125–139, <https://doi.org/10.1002/ppp.449>, 2003.
- Schuur, E. A., Abbott, B. W., Commane, R., Ernakovich, J., Euskirchen, E., Hugelius, G., Grosse, G., Jones, M., Koven, C., Leshyk, V., Lawrence, D., Lorant, M. M., Mauritz, M., Olefeldt, D., Natali, S., Rodenhizer, H., Salmon, V., Schädel, C., Strauss, J., Treat, C., and Turetsky, M.: Permafrost and Climate Change: Carbon Cycle Feedbacks From the Warming Arctic, *Annu. Rev. Env. Resour.*, 47, 343–371, <https://doi.org/10.1146/annurev-environ-012220-011847>, 2022.
- 515 Shiklomanov, N. I. and Nelson, F. E.: Active-Layer Mapping at Regional Scales: A 13-Year Spatial Time Series for the Kuparuk Region, North-Central Alaska, *Permafrost Periglac.*, 13, 219–230, <https://doi.org/10.1002/ppp.425>, 2002.
- 520 Shiklomanov, N. I., Streletskiy, D. A., Nelson, F. E., Hollister, R. D., Romanovsky, V. E., Tweedie, C. E., Bockheim, J. G., and Brown, J.: Decadal variations of active-layer thickness in moisture-controlled landscapes, Barrow, Alaska, *J. Geophys. Res.-Biogeo.*, 115, G00I04, <https://doi.org/10.1029/2009JG001248>, 2010.
- Smith, M. W. and Riseborough, D. W.: Permafrost monitoring and detection of climate change, *Permafrost Periglac.*, 7, 301–309, [https://doi.org/10.1002/\(SICI\)1099-1530\(199610\)7:4<301::AID-PPP231>3.0.CO;2-R](https://doi.org/10.1002/(SICI)1099-1530(199610)7:4<301::AID-PPP231>3.0.CO;2-R), 1996.
- 525 Smith, S. L., Wolfe, S. A., Riseborough, D. W., and Nixon, F. M.: Active-layer characteristics and summer climatic indices, Mackenzie Valley, Northwest Territories, Canada. *Permafrost Periglac.*, 20, 201–220, <https://doi.org/10.1002/ppp.651>, 2009.
- Smith, S. L., O’Neill, H. B., Isaksen, K., Noetzli, J., and Romanovsky, V. E.: The changing thermal state of permafrost, *Nat. Rev. Earth Environ.*, 3, 10–23, <https://doi.org/10.1038/s43017-021-00240-1>, 2022.
- Smith, S. L., Romanovsky, V. E., Isaksen, K., Nyland, K., Shiklomanov, N. I., Streletskiy, D. A., and Christiansen, H. H.: Permafrost (Arctic), in: State of the Climate in 2023, *Bull. Amer. Meteor. Soc.*, 105, S314–S317. <https://doi.org/10.1175/BAMS-D-24-0101.1>, 2024
- 530 Stefan, J.: Über die Theorie der Eisbildung, insbesondere über die Eisbildung im Polarmeere, *Ann. Phys.*, 278, 269–286, <https://doi.org/10.1002/andp.18912780206>, 1891.
- Streletskiy, D. A., Shiklomanov, N. I., and Nelson, F. E.: Spatial variability of permafrost active-layer thickness under contemporary and projected climate in northern Alaska, *Polar Geogr.*, 35, 95–116, <https://doi.org/10.1080/1088937X.2012.680204>, 2012.
- 535 Streletskiy, D., Noetzli, J., Smith, S. L., Vieira, G., Schoeneich, P., Hrbacek, F., and Irrgang, A. M.: Measurement Recommendations and Guidelines for the Global Terrestrial Network for Permafrost (GTN-P), Zenodo, <https://doi.org/10.5281/zenodo.5973079>, 2022.
- Walvoord, M. A., Kurylyk, B.L.: Hydrologic Impacts of Thawing Permafrost—A Review, *Vadose Zone J.*, 15, vzj2016-01, <https://doi.org/10.2136/vzj2016.01.0010>, 2016.



- Wang, C., Wang, Z., Kong, Y., Zhang, F., Yang, K., and Zhang, T.: Most of the Northern Hemisphere Permafrost Remains under Climate Change, *Sci. Rep.*, 9, 3295, <https://doi.org/10.1038/s41598-019-39942-4>, 2019.
- 540 Wang, K., Jafarov, E., and Overeem, I.: Sensitivity evaluation of the Kudryavtsev permafrost model, *Sci. Total Environ.*, 720, 137538, <https://doi.org/10.1016/j.scitotenv.2020.137538>, 2020.
- Way, R. G. and Lewkowicz, A. G.: Environmental controls on ground temperature and permafrost in Labrador, northeast Canada, *Permafrost Periglac.*, 29, 73–85, <https://doi.org/10.1002/ppp.1972>, 2018.
- 545 Wenhao, L., Ren, L., Tonghua, W., Xiaoqian, S., Xiaodong, W., Guojie, H., Lin, Z., Jimin, Y., Dong, W., Yao, X., Jianzong, S., Junjie, M., Shennig, W., and Yongping, Q.: Spatio-temporal variation in soil thermal conductivity during the freeze-thaw period in the permafrost of the Qinghai–Tibet Plateau in 1980–2020, *Sci. Total Environ.*, 913, 169654, <https://doi.org/10.1016/j.scitotenv.2023.169654>, 2024.
- Yin, G., Niu, F., Lin, Z., Luo, J., and Liu, M.: Performance comparison of permafrost models in Wudaoliang Basin, Qinghai-Tibet plateau, China, *J. Mt. Sci.*, 13, 1162–1173, <https://doi.org/10.1007/s11629-015-3745-x>, 2016.
- 550 Zhao, S. P., Nan, Z. T., Huang, Y. B., and Zhao, L.: The Application and Evaluation of Simple Permafrost Distribution Models on the Qinghai–Tibet Plateau, *Permafrost Periglac.*, 28, 391–404, <https://doi.org/10.1002/ppp.1939>, 2017.
- Zhao, L., Zou, D., Hu, G., Wu, T., Du, E., Liu, G., Xiao, Y., Li, R., Pang, Q., Qiao, Y., Wu, X., Sun, Z., Xing, Z., Sheng, Y., Zhao, Y., Shi, J., Xie, C., Wang, L., Wang, C., and Cheng, G.: A synthesis dataset of permafrost thermal state for the Qinghai–Tibet (Xizang) Plateau, China, *Earth Syst. Sci. Data*, 13, 4207–4218, <https://doi.org/10.5194/essd-13-4207-2021>, 2021.
- 555 Zorigt, M., Kwadijk, J., Van Beek, E., and Kenner, S.: Estimating thawing depths and mean annual ground temperatures in the Khuvsgul region of Mongolia, *Environ. Earth Sci.*, 75, 897, <https://doi.org/10.1007/s12665-016-5687-1>, 2016.